SCIENCE CHINA
Information Sciences

• RESEARCH PAPER •

January 2022, Vol. 65 112302:1–112302:11
https://doi.org/10.1007/s11432-020-3230-4

On the uniqueness of virtual substrate for metasurface in a dielectric half-space

Xiaobo LIU[1,2], Wei XUE[1], Xiaoming CHEN[1*], Anxue ZHANG[1*], Qiang CHENG[3] & Zongben XU[2*]

[1]*School of Information and Communications Engineering, Xi'an Jiaotong University, Xi'an* 710049*, China;*
[2]*School of Mathematics and Statistics, Xi'an Jiaotong University, Xi'an* 710049*, China;*
[3]*State Key Laboratory of Millimeter Waves and School of Electrical Engineering, Southeast University, Nanjing* 210096*, China*

Received 2 November 2020/Revised 4 March 2021/Accepted 23 March 2021/Published online 23 December 2021

Abstract In this paper, we study the uniqueness of a virtual substrate for periodic metallic elements in a dielectric half-space. When the periodic metallic elements are placed at the interface of different substrates, they can be regarded to be embedded into a virtual substrate whose thickness approaches zero. However, the process of the mathematical limit of the thickness seems to be independent of the choice of the virtual substrate. Thereby, it is necessary to verify whether the arbitrary virtual substrate holds for the case. It is theoretically verified that the permittivity of the virtual substrate should be unique in order to satisfy the physical boundary condition of the periodic metallic elements. The root of the phenomenon is that the mathematical limit gives the alternative means to approach the actual physical situation, but the actual physical situation determines the way how the mathematical limit approaches zero. Finally, for comparison, two different virtual substrates are designed to validate the theory, for alternative substrate, incidence angle, and metallic elements. Besides, the finding can also be used to simplify the analysis and design of the metasurface by converting the periodic metallic elements in a dielectric half-space to the same periodic metallic elements in a uniform substrate.

Keywords virtual substrate, periodic metallic elements, mathematical limit, relative permittivity, boundary condition

Citation Liu X B, Xue W, Chen X M, et al. On the uniqueness of virtual substrate for metasurface in a dielectric half-space. Sci China Inf Sci, 2022, 65(1): 112302, https://doi.org/10.1007/s11432-020-3230-4

1 Introduction

The metasurface is usually a kind of two-dimensional periodic metallic element printed on the substrates [1–4]. Different from the traditional electromagnetic materials, the resonant characteristic of the sub-wavelength metallic elements plays an important role for achieving various functionalities of the metasurface, such as polarization converters [5–8], spoof surface plasmon polariton couplers [9–11], orbital angular momentum generators [12, 13], and cloaks [14–17]. Besides numerous designs of metasurfaces, efforts have also been exerted to refine the theories of the metasurface. Specifically, when the period of the metallic elements is much smaller than the operation wavelength, the periodic metallic elements can be handled as a homogenized surface [18, 19]. Thereby, the key is to establish corresponding boundary condition for the periodic metallic elements. In the previous studies, many methods have been developed to solve the boundary condition at the interface of different substrates [20–26]. Although these methods make great progress in the theoretical study, there is still room for improvement.

Specifically, the metasurface can be physically regarded as a homogenized surface with a specific boundary condition in a dielectric half-space. Owing to the influence of the dielectric half-space for the secondary radiation of the metasurface, it is hard to analytically derive its boundary condition, especially for metasurface with complex metallic elements [21, 22]. In our previous work, a virtual substrate is

* Corresponding author (email: xiaoming.chen@mail.xjtu.edu.cn, anxuezhang@mail.xjtu.edu.cn, zbxu@mail.xjtu.edu.cn)

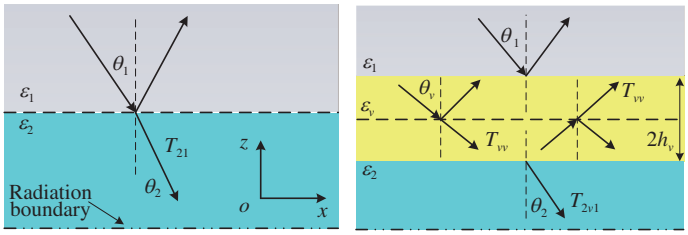

Figure 1 (Color online) Periodic metallic elements (a) at the interface of substrates 1 and 2, and (b) in the virtual substrate.

mathematically introduced for periodic metallic elements in a dielectric half-space, which can convert the solution of the metasurface in a dielectric half-space into that in a homogenized virtual substrate [27]. Despite this, an important open problem is about the relative permittivity of the virtual substrate. Specifically, in order to make the updated model with virtual substrate boil down to the original physical model, the thickness of the virtual substrate is required to approach zero. However, the mathematical limit process seems to be independent of the virtual substrate, which means that the virtual substrate can be arbitrarily given. The problem concerns how to accurately convert the solution of the metasurface in a dielectric half-space into that in a virtual substrate. If the generic problem can be solved, only the periodic metallic elements in the homogenized substrate need to be theoretically considered, so that the solution of the boundary condition of the periodic metallic elements can be greatly simplified. Thus, it is necessary to verify whether an arbitrary zero-thickness virtual substrate can convert the solution of metasurface in a dielectric half-space into that in a virtual substrate.

In this paper, we study an almost zero-thickness virtual substrate for periodic metallic elements in a dielectric half-space. It is theoretically verified that, when a zero-thickness virtual substrate is introduced to cover the periodic metallic elements, the permittivity of the virtual substrate must be unique to satisfy the original boundary condition. Once the permittivity of the virtual substrate deviates from a specific value, the updated model with the virtual substrate is no longer valid. Finally, two different virtual substrates for comparison are designed and simulated to support the proposed theory, regardless of the substrate, incidence angle, and metallic elements. The theory not only demonstrates the uniqueness of the virtual substrate but also converts the solution of periodic metallic elements at the interface into that of the same periodic metallic elements in a homogenized substrate, which can greatly simplify the theoretical analysis and design of the boundary condition for the metasurface.

The rest of the paper is organized as follows. In Subsection 2.1, the permittivity of the virtual substrate is verified to be unique for periodic isotropic metallic elements. In Subsection 2.2, the permittivity of the virtual substrate is verified to be also unique for periodic anisotropic metallic elements. For comparison, two kinds of virtual substrates are adopted to verify the theory in Section 3. Finally, the conclusion is drawn in Section 4.

2 Theoretical analysis

As shown in Figure 1(a), the periodic metallic elements are placed at the interface of substrates 1 and 2, where ε_1 and ε_2 are assumed to be the relative permittivity of the substrates 1 and 2, respectively. Here, the period of the metallic elements is assumed to be smaller than the operation wavelength. Thereby, the periodic metallic elements can be handled as a uniform surface. When the perpendicular polarized wave (TE) and parallel polarized wave (TM) waves $\boldsymbol{E}_{\rm inc}$ obliquely impinge on the periodic metallic elements, the transmitted wave will exist in substrate 2 with the corresponding tangential transmission matrix T_{21}. Although many methods have been developed to directly solve the periodic metallic elements, the problem can be tackled in another way. Specifically, as shown in Figure 1(b), the periodic metallic elements can be first placed in the virtual substrate with a relative permittivity of ε_v and a thickness of $2h_v$ [27]. As the thickness approaches zero, the updated model in Figure 1(b) boils down to the original one in Figure 1(a). Thus, the solution of the periodic metallic elements in a dielectric half-space can be converted into that of the same periodic metallic elements in a uniform substrate, which can greatly simplify the study of the periodic metallic elements.

Although the above method has been previously verified, an important problem about the value of ε_v remains to be solved. No matter which value of ε_v is given, the updated model in Figure 1(b) will boil

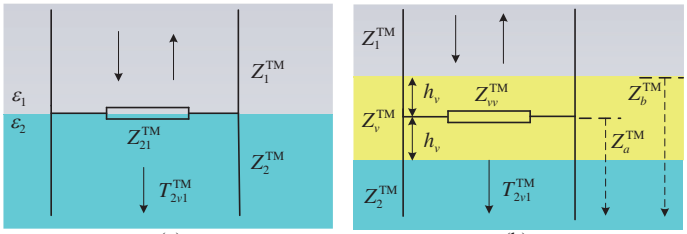

Figure 2 (Color online) Transmission-lie model for the periodic isotropic metallic elements (a) at the interface of substrates 1 and 2, and (b) in the virtual substrate.

down to the original one in Figure 1(a) with the mathematical limit $h_v \to 0$. Thereby, the mathematical limit seems to be independent of the virtual substrate which can be arbitrarily given. Considering that $\varepsilon_v = (\varepsilon_1 + \varepsilon_2)/2$ is analogously adopted for the virtual substrate directly without rigorous discussion in the previous work, it is necessary to verify whether other zero-thickness virtual substrates are also valid for the periodic metallic elements as the original one. Thus, the uniqueness of the virtual substrate will be studied for the virtual substrate in the sequel.

2.1 Uniqueness of virtual substrate for periodic isotropic metallic elements

The study is first conducted for periodic isotropic metallic elements. In this case, there will not be polarization conversion for the TE or TM incident wave, the tangential electrical and magnetic fields with the normal propagation constant are regarded as the voltage and current, respectively. In this case, the periodic isotropic metallic elements can be handled as parallel scalar impedance in the transmission-line model, and the substrates can be similarly handled as transmission lines with corresponding characteristic impedances. For brevity, the solution is only conducted for the TM wave here, while the TE wave case can be handled in a similar way.

Specifically, as shown in Figure 2, for the obliquely incident TM waves, $Z_{21}^{\text{TM-TM}}$ and $Z_{vv}^{\text{TM-TM}}$ are assumed to denote the parallel impedances of the periodic isotropic metallic elements in the dielectric half-space and the virtual substrate, respectively. Thereby, the corresponding transmission coefficient can be derived according to the transmission-line theory as follows.

First, as shown in Figure 2(a), the tangential transmission coefficient T_{21}^{TM} is given by

$$T_{21}^{\mathrm{TM}} = \frac{Z_{21}^{\text{TM-TM}} \| Z_2^{\text{TM-TM}} - Z_1^{\text{TM-TM}}}{Z_{21}^{\text{TM-TM}} \| Z_2^{\text{TM-TM}} + Z_1^{\text{TM-TM}}} + 1 \tag{1}$$

with

$$\frac{1}{Z_{21}^{\text{TM-TM}} \| Z_2^{\text{TM}}} = \frac{1}{Z_{21}^{\text{TM-TM}}} + \frac{1}{Z_2^{\mathrm{TM}}} = \frac{1}{Z_{21}^{\text{TM-TM}}} + \frac{\sqrt{\varepsilon_0 \varepsilon_2}}{\sqrt{\mu_0} \cos\theta_2}, \tag{2}$$

where $Z_1^{\mathrm{TM}} = Z_1 \cos\theta_1$ and $Z_2^{\mathrm{TM}} = Z_2 \cos\theta_2$ are the TM wave impedances of substrates 1 and 2 respectively, and θ_2 is the transmission angle in substrate 2.

Next, as shown in Figure 2(b), the tangential transmission coefficient T_{2v1}^{TM} is solved as

$$T_{2v1}^{\mathrm{TM}} = \frac{Z_b^{\mathrm{TM}} - Z_1^{\mathrm{TM}}}{Z_b^{\mathrm{TM}} + Z_1^{\mathrm{TM}}} + 1 \tag{3}$$

with

$$\begin{aligned} Z_a^{\mathrm{TM}} &= Z_v^{\mathrm{TM}} \frac{Z_2^{\mathrm{TM}} + \mathrm{j} Z_v^{\mathrm{TM}} \tan(\sqrt{\varepsilon_v} k_0 \cos\theta_v h_v)}{Z_v^{\mathrm{TM}} + \mathrm{j} Z_2^{\mathrm{TM}} \tan(\sqrt{\varepsilon_v} k_0 \cos\theta_v h_v)}, \\ Z_b^{\mathrm{TM}} &= Z_v^{\mathrm{TM}} \frac{Z_{vv}^{\text{TM-TM}} \| Z_a^{\mathrm{TM}} + \mathrm{j} Z_v^{\mathrm{TM}} \tan(\sqrt{\varepsilon_v} k_0 \cos\theta_v h_v)}{Z_v^{\mathrm{TM}} + \mathrm{j} (Z_{vv}^{\text{TM-TM}} \| Z_a^{\mathrm{TM}}) \tan(\sqrt{\varepsilon_v} k_0 \cos\theta_v h_v)}, \end{aligned} \tag{4}$$

where Z_1^{TM} and Z_v^{TM} are the TM wave impedances for the substrate 1 and the virtual substrate, respectively; Z_a^{TM} and Z_b^{TM} are the equivalent TM impedances at the lower interface of the periodic metallic elements and the upper interface of the virtual substrate, respectively; $\sqrt{\varepsilon_v} k_0 \cos\theta_v$ is the normal propagation wave number in the virtual substrate for tangential fields; θ_v is the transmission angle in the virtual substrate and satisfies the following refraction law:

$$\sqrt{\varepsilon_v} \sin\theta_v = \sqrt{\varepsilon_1} \sin\theta_1 = \sqrt{\varepsilon_2} \sin\theta_2. \tag{5}$$

Finally, in order to turn the updated model in Figure 2(b) to the original one in Figure 2(a), the thickness $2h_v$ of the virtual substrate is required to be close to zero. In this case, T_{2v1}^{TM} will satisfy the following equation:

$$\lim_{h_v\to 0} T_{2v1}^{\mathrm{TM}} = \frac{Z_{vv}^{\mathrm{TM\text{-}TM}} \| Z_2^{\mathrm{TM}} - Z_1^{\mathrm{TM}}}{Z_{vv}^{\mathrm{TM\text{-}TM}} \| Z_2^{\mathrm{TM}} + Z_1^{\mathrm{TM}}} + 1. \tag{6}$$

By comparing (6) and (1), the following relationship can be deduced easily:

$$Z_{21}^{\mathrm{TM\text{-}TM}} = Z_{vv}^{\mathrm{TM\text{-}TM}}, \quad T_{21}^{\mathrm{TM}} = \lim_{h_v\to 0} T_{2v1}^{\mathrm{TM}}. \tag{7}$$

Similarly, the corresponding relationship for the TE wave is given as follows:

$$Z_{21}^{\mathrm{TE\text{-}TE}} = Z_{vv}^{\mathrm{TE\text{-}TE}}, \quad T_{21}^{\mathrm{TE}} = \lim_{h_v\to 0} T_{2v1}^{\mathrm{TE}}. \tag{8}$$

Eqs. (7) and (8) can be analyzed from the following two aspects. On one hand, as the thickness of the virtual substrate approaches zero, the periodic metallic elements in Figures 1(a) and (b) share the same reflection (transmission) characteristics. Thereby, the two kinds of scalar impedances are always equal to each other. On the other hand, when the periodic metallic elements are placed at the interface of substrates 1 and 2, the reflection and transmission characteristics represented by $Z_{21}^{\mathrm{TM\text{-}TM}}$ and $Z_{21}^{\mathrm{TE\text{-}TE}}$ can be determined a priori. However, there is no doubt that Z_{vv} will vary with the relative permittivity ε_v of the virtual substrate. Thus, in order to avoid contradiction, the relative permittivity ε_v of the virtual substrate cannot be arbitrarily given, and more importantly, should be unique.

2.2 Uniqueness of virtual substrate for periodic anisotropic metallic elements

After verifying the uniqueness of the virtual substrate for periodic isotropic metallic elements, it remains to solve the problem for periodic anisotropic metallic elements. However, the periodic anisotropic metallic elements cannot be handled as scalar impedance due to potential polarized conversion, so that the traditional transmission-line theory cannot be directly applied to anisotropic metallic elements. In this case, we resort to the tangential network transmission theory to analyze the problem.

First, for the model in Figure 1(a), the tangential transmission matrix T_{21} is first expressed as the following equation [24]:

$$\boldsymbol{E}_{\mathrm{tot}}^{\tan} = T_{21}\boldsymbol{E}_{\mathrm{inc}}^{\tan} = (U - Z_{\|,21}I_{21}^{\mathrm{sub}})t_{21}\boldsymbol{E}_{\mathrm{inc}}^{\tan} \tag{9}$$

with

$$\begin{aligned} t_{21} &= \begin{bmatrix} 2Z_2^{\mathrm{TM}}/(Z_2^{\mathrm{TM}} + Z_1^{\mathrm{TM}}) & 0 \\ 0 & 2Z_2^{\mathrm{TE}}/(Z_2^{\mathrm{TE}} + Z_1^{\mathrm{TE}}) \end{bmatrix}, \\ Z_{\|,21} &= \begin{bmatrix} Z_1^{\mathrm{TM}}Z_2^{\mathrm{TM}}/(Z_1^{\mathrm{TM}} + Z_2^{\mathrm{TM}}) & 0 \\ 0 & Z_1^{\mathrm{TE}}Z_2^{\mathrm{TE}}/(Z_1^{\mathrm{TE}} + Z_2^{\mathrm{TE}}) \end{bmatrix}, \end{aligned} \tag{10}$$

where $\boldsymbol{E}_{\mathrm{tot}}^{\tan}$ and $\boldsymbol{E}_{\mathrm{inc}}^{\tan}$ are the total and incident tangential electric field at the interface, respectively; U is a two-dimensional unit matrix; t_{21} is the tangential transmission matrix from the traditional Fresnel's formula; I_{21}^{sub} describes the mathematical relationship between the external excited field $t_{21}\boldsymbol{E}_{\mathrm{inc}}^{\tan}$ and the induced surface current density $\boldsymbol{J}$. Further, the total tangential electric field $\boldsymbol{E}_{\mathrm{tot}}^{\tan}$ can also be related to the induced surface current density $\boldsymbol{J}$ through the following equations:

$$\boldsymbol{E}_{\mathrm{tot}}^{\tan} = Z_{21}\boldsymbol{J} = Z_{21}I^{\mathrm{sub}}t_{21}\boldsymbol{E}_{\mathrm{inc}}^{\tan} \tag{11}$$

with

$$Z_{21} = \begin{bmatrix} Z_{21}^{\mathrm{TM\text{-}TM}} & Z_{21}^{\mathrm{TM\text{-}TE}} \\ Z_{21}^{\mathrm{TE\text{-}TM}} & Z_{21}^{\mathrm{TE\text{-}TE}} \end{bmatrix}, \tag{12}$$

where Z_{21} is defined as the surface impedance matrix of the periodic metallic elements at the interface. In this case, Z_{21} completely determines the reflection and transmission characteristics of the periodic metallic elements at the interface. By comparing (9) and (11), the tangential transmission matrix T_{21} can be rewritten as

$$T_{21}^{-1} = (Z_{21}I^{\mathrm{sub}}t_{21})^{-1} = t_{21}^{-1}(U + Z_{\|,21}Z_{21}^{-1}) \tag{13}$$

with

$$I_{21}^{\text{sub}} = (Z_{21} + Z_{\parallel,21})^{-1}. \tag{14}$$

Eq. (13) establishes the mathematical relationship between the tangential transmission matrix and the surface impedance matrix for periodic anisotropic metallic elements as (1).

Then, for the updated model in Figure 1(b), the metasurface can be regarded as a quad-layer structure with the total tangential transmission matrix T_{2v1}. As the thickness $2h_v$ of the virtual substrate approaches zero, T_{2v1} can be similarly derived according to (13) [27]. Here, for convenience, the expression of T_{2v1} can be rewritten as follows:

$$\lim_{h_v \to 0} 2T_{2v1}^{-1} = U - 2Z_{c,1}Z_{c,v}^{-1} + Z_{c,1}Z_{c,2}^{-1} + 2Z_{c,1}Z_{c,v}^{-1}T_{vv}^{-1} \tag{15}$$

with

$$Z_{c,v} = \frac{Z_0}{\sqrt{\varepsilon_v}} \begin{bmatrix} 0 & -\cos\theta_v \\ 1/\cos\theta_v & 0 \end{bmatrix} = \begin{bmatrix} 0 & -Z_v^{\text{TM}} \\ Z_v^{\text{TE}} & 0 \end{bmatrix}, \tag{16}$$

where $Z_{c,1}$ and $Z_{c,2}$ are similarly defined as $Z_{c,v}$. T_{vv} is the tangential transmission matrix of the periodic metallic elements in the virtual substrate. Further, the tangential transmission matrix T_{vv} can also be expressed with the surface impedance matrix as (13)

$$T_{vv}^{-1} = t_{vv}^{-1}(U + Z_{\parallel,vv}Z_{vv}^{-1}) = U + Z_{\parallel,vv}Z_{vv}^{-1} \tag{17}$$

with

$$Z_{\parallel,vv} = \frac{1}{2} \begin{bmatrix} Z_v^{\text{TM}} & 0 \\ 0 & Z_v^{\text{TE}} \end{bmatrix}, \quad Z_{vv} = \begin{bmatrix} Z_{vv}^{\text{TM-TM}} & Z_{vv}^{\text{TM-TE}} \\ Z_{vv}^{\text{TE-TM}} & Z_{vv}^{\text{TE-TE}} \end{bmatrix}, \tag{18}$$

where $Z_{\parallel,vv}$ is defined in a similar way as $Z_{\parallel,21}$; Z_{vv} is the impedance matrix of the periodic metallic elements in the virtual substrate. In this case, substituting (17) into (15) yields the following equation:

$$\lim_{h_v \to 0} 2T_{2v1}^{-1} = U + Z_{c,1}Z_{c,2}^{-1} + 2Z_{c,1}Z_{c,v}^{-1}Z_{\parallel,vv}Z_{vv}^{-1}. \tag{19}$$

Finally, according to the theory, as the thickness of the virtual substrate approaches zero, the total tangential transmission matrix T_{2v1} also gradually approaches T_{21}. By comparing (19) and (13), one obtains the following equation:

$$Z_{21} = Z_{vv}. \tag{20}$$

Eq. (20) can be regarded as the extension of (6) and (7) to the periodic anisotropic metallic elements. More importantly, it verifies that, in order to make the two models in Figure 1 share the same reflection (transmission) characteristics, the virtual substrate cannot be arbitrarily given and must satisfy a specific condition. Otherwise, Z_{vv} will vary with the relative permittivity ε_v of the virtual substrate while Z_{21} keeps unchanged. This will result in contradiction with (20). Thus, the mathematical limit seems to be independent of the virtual substrate, but the virtual substrate is actually unique.

In fact, the phenomenon demonstrates that the boundary condition of the periodic metallic elements determines the way how the mathematical limit approaches the actual physical situation. An example can be used for clarification, i.e., when the Fourier transformation is used to solve the Helmholtz's equation with the Dirac's source, there will be two singularities in the integral path. In this case, the treatment of the two singularities is related to the mathematical limit of the integral path, which will result in different solutions. Although these solutions all satisfy the Helmholtz's equation, only one is the right solution to the problem according to the radiation boundary condition. Thus, the mathematical limit gives an alternative means to approach the actual physical situation, while the actual physical situation determines the way how the mathematical limit approaches it.

3 Verification of the proposed theory

According to the theory, the following relationship between T_{21} and T_{vv} holds only when the virtual substrate is correctly given

$$2T_{21}^{-1} = \lim_{h_v \to 0} 2T_{2v1}^{-1} = U - 2Z_{c,1}Z_{c,v}^{-1} + Z_{c,1}Z_{c,2}^{-1} + 2Z_{c,1}Z_{c,v}^{-1}T_{vv}^{-1}. \tag{21}$$

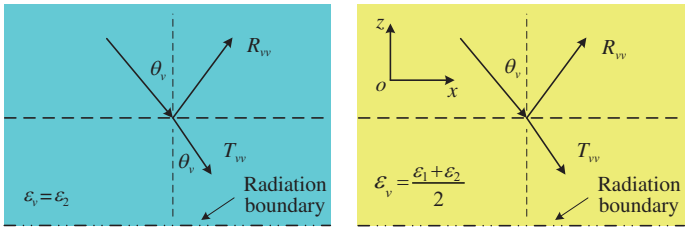

Figure 3 (Color online) Oblique incidence on the periodic metallic elements (a) in the virtual substrate with $\varepsilon_v = (\varepsilon_1 + \varepsilon_2)/2$, and (b) in the virtual substrate with $\varepsilon_v = \varepsilon_2$.

When T_{21} is given a prior, T_{vv} can be analytically calculated as (21) or obtained via numerical simulation. However, when the virtual substrate is not correctly given, there will be an inevitable deviation between the theoretical and simulated T_{vv}. Thus, the verification will be conducted for T_{vv} in terms of two different virtual substrates.

First, T_{21} can be derived from the high frequency structure simulator (HFSS) software simulation, as shown in Figure 1(a). Considering that the simulated transmission matrix becomes invalid due to the existence of radiation boundary condition, the tangential transmission matrix T_{21} can be derived as follows:

$$T_{21} = R_{21} + U \tag{22}$$

with

$$R_{21} = \begin{bmatrix} R_{21}^{11} & R_{21}^{12} \\ R_{21}^{21} & R_{21}^{22} \end{bmatrix} = \begin{bmatrix} R_{21}^{\text{TM-TM}} & R_{21}^{\text{TM-TE}}\cos\theta_1 \\ R_{21}^{\text{TE-TM}}\cos\theta_1 & R_{21}^{\text{TE-TE}} \end{bmatrix}, \tag{23}$$

where R_{21} is the tangential reflection matrix at the interface; $R_{21}^{\text{TM-TM}}$, $R_{21}^{\text{TM-TE}}$, $R_{21}^{\text{TE-TM}}$, and $R_{21}^{\text{TE-TE}}$ are the simulated reflection coefficients; Eq. (22) is required by the continuity of tangential electrical fields.

Then, based on the theoretically derived T_{21}, the theoretical T_{vv} can be solved through (21). For the convenience of comparison, the theoretical T_{vv} is converted into the corresponding reflection matrix R as follows:

$$R = \begin{bmatrix} R_{vv}^{\text{TM-TM}} & R_{vv}^{\text{TM-TE}} \\ R_{vv}^{\text{TE-TM}} & R_{vv}^{\text{TE-TE}} \end{bmatrix} = \begin{bmatrix} R_{vv}^{11} & R_{vv}^{12}/\cos\theta_v \\ R_{vv}^{21}\cos\theta_v & R_{vv}^{22} \end{bmatrix} \tag{24}$$

with

$$R_{vv} = \begin{bmatrix} R_{vv}^{11} & R_{vv}^{12} \\ R_{vv}^{21} & R_{vv}^{22} \end{bmatrix} = T_{vv} - U, \tag{25}$$

where R_{vv} is the tangential reflection matrix in the virtual substrate; $R_{vv}^{\text{TM-TM}}$, $R_{vv}^{\text{TM-TE}}$, $R_{vv}^{\text{TE-TM}}$, and $R_{vv}^{\text{TE-TE}}$ are the reflection coefficients in the virtual substrate.

Besides, R (T_{vv}) can also be obtained by simulating the periodic metallic elements in two different virtual substrates. As shown in Figure 3, the first kind of virtual substrate is analogously fixed with $\varepsilon_v = (\varepsilon_1 + \varepsilon_2)/2$ in [27], while the second kind of virtual substrate is arbitrarily selected with $\varepsilon_v = \varepsilon_2$. Finally, by comparing the consistency between the theoretical and simulated R in terms of the two different virtual substrates, we can verify the uniqueness of the virtual substrate.

3.1 Periodic isotropic metallic elements

Figure 4 shows an isotropic metallic element (i.e., unit cell) that will be used for the verification. The geometric parameters of the unit cell are fixed as $p = 4.5$ mm, $d = 1.8$ mm, and $q = 0.2$ mm. According to the above discussion, the periodic metallic elements are first simulated to obtain the tangential transmission matrix T_{21}. In the HFSS simulation, the x- and y-directed boundaries of the unit cell are set to be periodic; the TE and TM waves obliquely impinge on the periodic isotropic metallic elements. For convenience and without loss of generality, substrate 1 is set as air ($\varepsilon_1 = 1$). After determining T_{21}, the theoretical R (T_{vv}) can be directly solved through (21) and (24), and the simulated R (T_{vv}) can be obtained similarly as T_{21} for the periodic metallic elements in the virtual substrate.

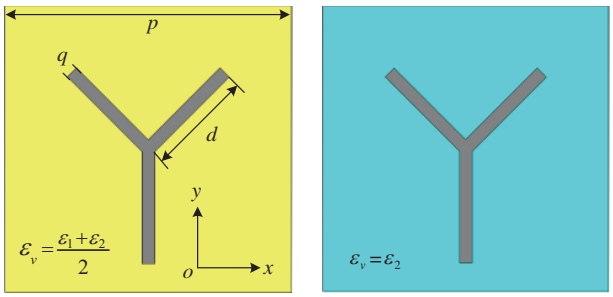

Figure 4 (Color online) Periodic isotropic metallic elements (a) in the virtual substrate with $\varepsilon_v = (\varepsilon_1 + \varepsilon_2)/2$, and (b) in the virtual substrate with $\varepsilon_v = \varepsilon_2$.

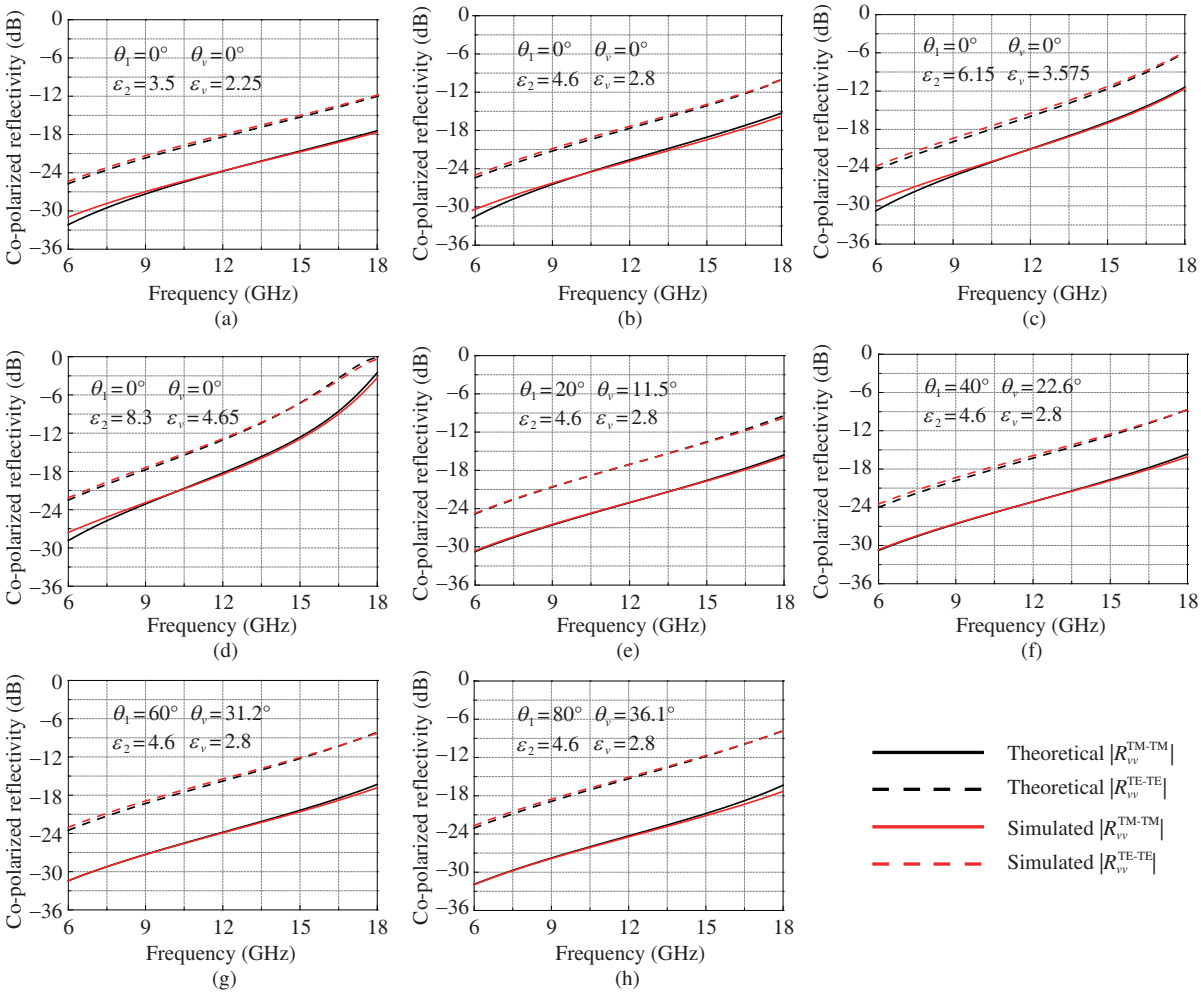

Figure 5 (Color online) Theoretical and simulated reflection coefficients for the virtual substrate with relative permittivity of $\varepsilon_v = (\varepsilon_1 + \varepsilon_2)/2$: (a)–(d) at normal incidence with varying substrate 2 and (e)–(h) at oblique incidence with fixed substrate 2.

When the relative permittivity of the virtual substrate is set as $\varepsilon_v = (\varepsilon_1 + \varepsilon_2)/2 = (1 + \varepsilon_2)/2$, Figure 5 shows the theoretical and simulated R for the periodic isotropic metallic elements in the virtual substrate. Due to the symmetry of the unit cell, only the co-polarized reflection coefficients are plotted in each figure. In Figures 5(a)–(d), when the incidence angle θ_1 is set as 0° and the relative permittivity ε_2 varies from 3.5 to 8.3, the theoretical results match well to the simulated ones. Further, in Figures 5(e)–(h), when the relative permittivity ε_2 is set as 4.6 and incidence angle θ_1 varies from 20° to 80°, there is still good consistency between the theoretical and simulated R. Thus, the theoretical results match well to the simulated ones in the case of $\varepsilon_v = (\varepsilon_1 + \varepsilon_2)/2 = (1 + \varepsilon_2)/2$ for arbitrary relative permittivity ε_2 and

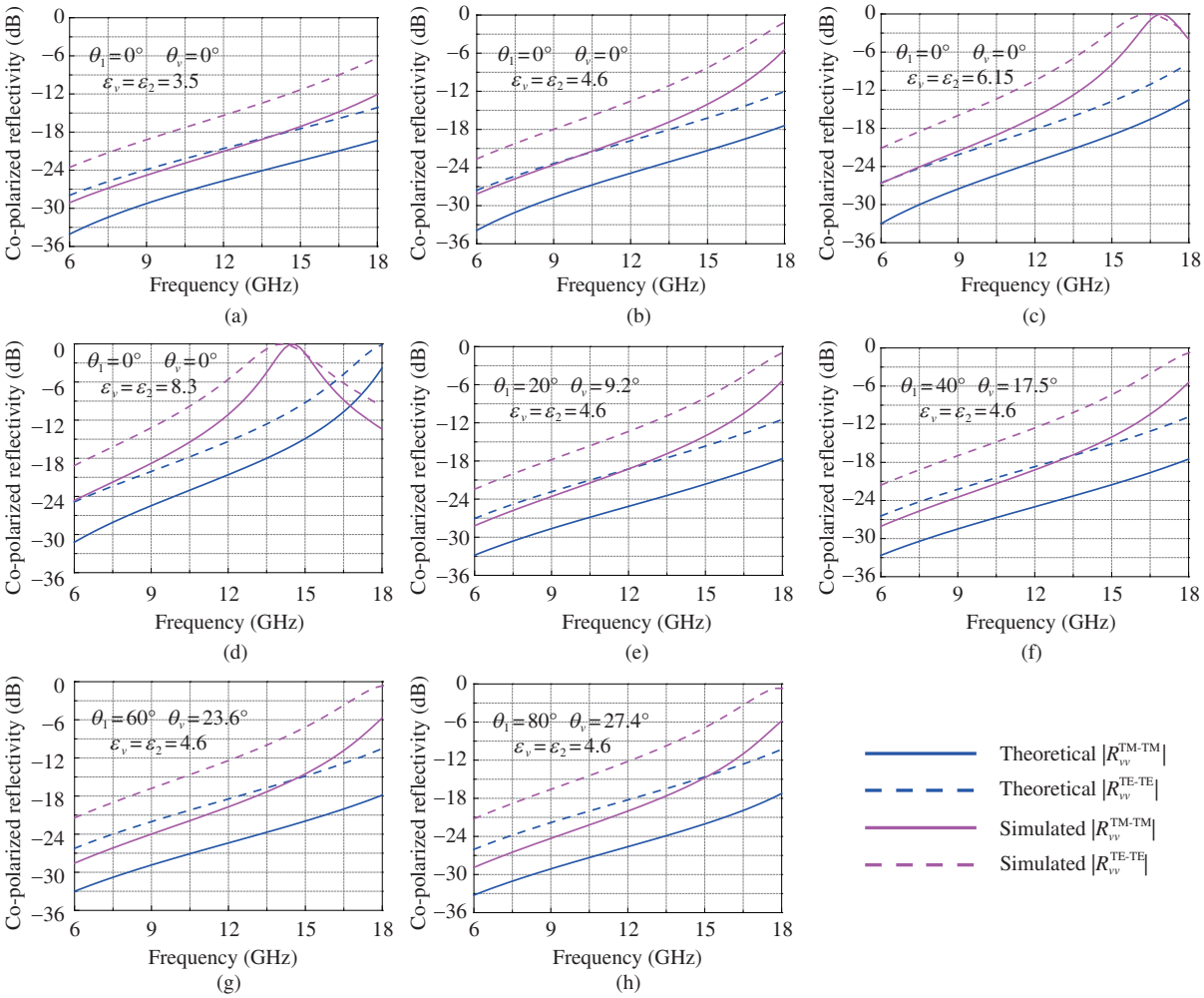

Figure 6 (Color online) Theoretical and simulated reflection coefficients for the virtual substrate with the relative permittivity of $\varepsilon_v = \varepsilon_2$: (a)–(d) at normal incidence with varying substrate 2 and (e)–(h) at oblique incidence with fixed substrate 2.

incidence angle θ_1.

As the above discussion, in order to verify the uniqueness of the virtual substrate, more simulations are made for comparisons, as shown in Figure 6. In these simulations, the relative permittivity of the virtual substrate is fixed as $\varepsilon_v = \varepsilon_2$. It can be observed that, no matter how the relative permittivity ε_2 and incident angle θ_1 change, the theoretical results significantly deviate from the simulated ones. The main reason is that the updated model with the virtual substrate of $\varepsilon_v = \varepsilon_2$ cannot provide the same boundary condition for the periodic metallic elements as the original model. Thus, these simulations support the proposed theory that the virtual substrate should be unique for the periodic isotropic metallic elements.

3.2 Periodic anisotropic metallic elements

After verifying the proposed theory for the periodic isotropic metallic elements, the case of the periodic anisotropic metallic elements remains to be validated. As shown in Figure 7, the designed unit cell is composed of double L-shaped metallic elements with the geometric parameters $p = 4.5$ mm, $d = 1.8$ mm, and $q = 0.2$ mm. As before, the HFSS software is adopted to simulate the tangential transmission matrix T_{21}. In the simulation, the substrate 1 is still fixed as air ($\varepsilon_1 = 1$) while the substrate 2 is variable. After deriving the theoretical R (T_{vv}) from T_{21}, similar simulation will be conducted to solve R (T_{vv}) for the periodic anisotropic metallic elements in two different virtual substrates. By comparing the theoretical and simulated R in terms of different virtual substrates, it can be used to determine whether the proposed theory is correct.

Figure 8 shows the theoretical and simulated R for the periodic anisotropic metallic elements in the virtual substrate with a relative permittivity of $\varepsilon_v = (\varepsilon_1 + \varepsilon_2)/2 = (1 + \varepsilon_2)/2$. Owing to the anisotropy

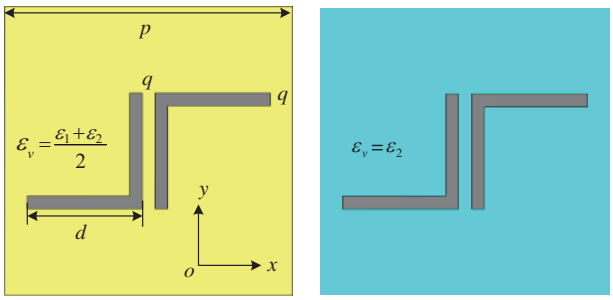

Figure 7 (Color online) Periodic anisotropic metallic elements (a) in the virtual substrate with $\varepsilon_v = (\varepsilon_1 + \varepsilon_2)/2$, and (b) in the virtual substrate with $\varepsilon_v = \varepsilon_2$.

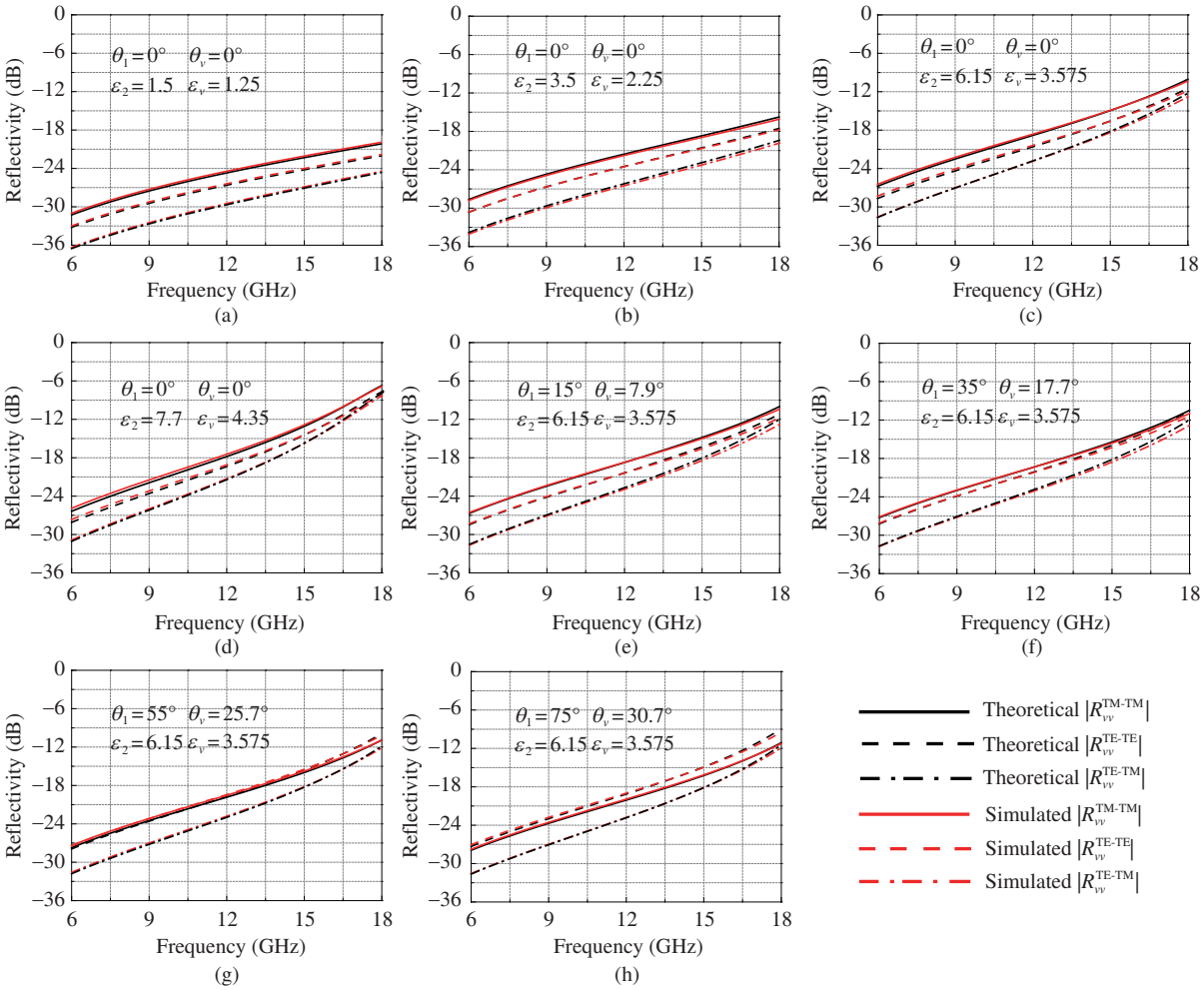

Figure 8 (Color online) Theoretical and simulated reflection coefficients for the virtual substrate with relative permittivity of $\varepsilon_v = (\varepsilon_1 + \varepsilon_2)/2$: (a)–(d) at normal incidence with varying substrate 2 and (e)–(h) at oblique incidence with fixed substrate 2.

of the metallic elements, the cross-polarized reflection coefficients are no longer equal to zero and satisfy the relationship $R_{vv}^{\text{TM-TE}} = R_{vv}^{\text{TE-TM}}$. This is verified by the theory as well as simulation. Similarly, the incidence angle θ_1 is set as 0° and the relative permittivity ε_2 varies in Figures 8(a)–(d), while the relative permittivity ε_2 is set as 6.15 and the incidence angle θ_1 varies in Figures 8(e)–(h). In this case, the theoretical results always match well with the simulated ones, regardless of the relative permittivity ε_2 and incidence angle θ_1. Thus, it can be concluded that $(\varepsilon_1+\varepsilon_2)/2$ should be very close to the accurate relative permittivity ε_v of the virtual substrate (Note that, due to the complexity of the metallic elements, it is hard to solve the exact relative permittivity of the virtual substrate which may depend on the actual

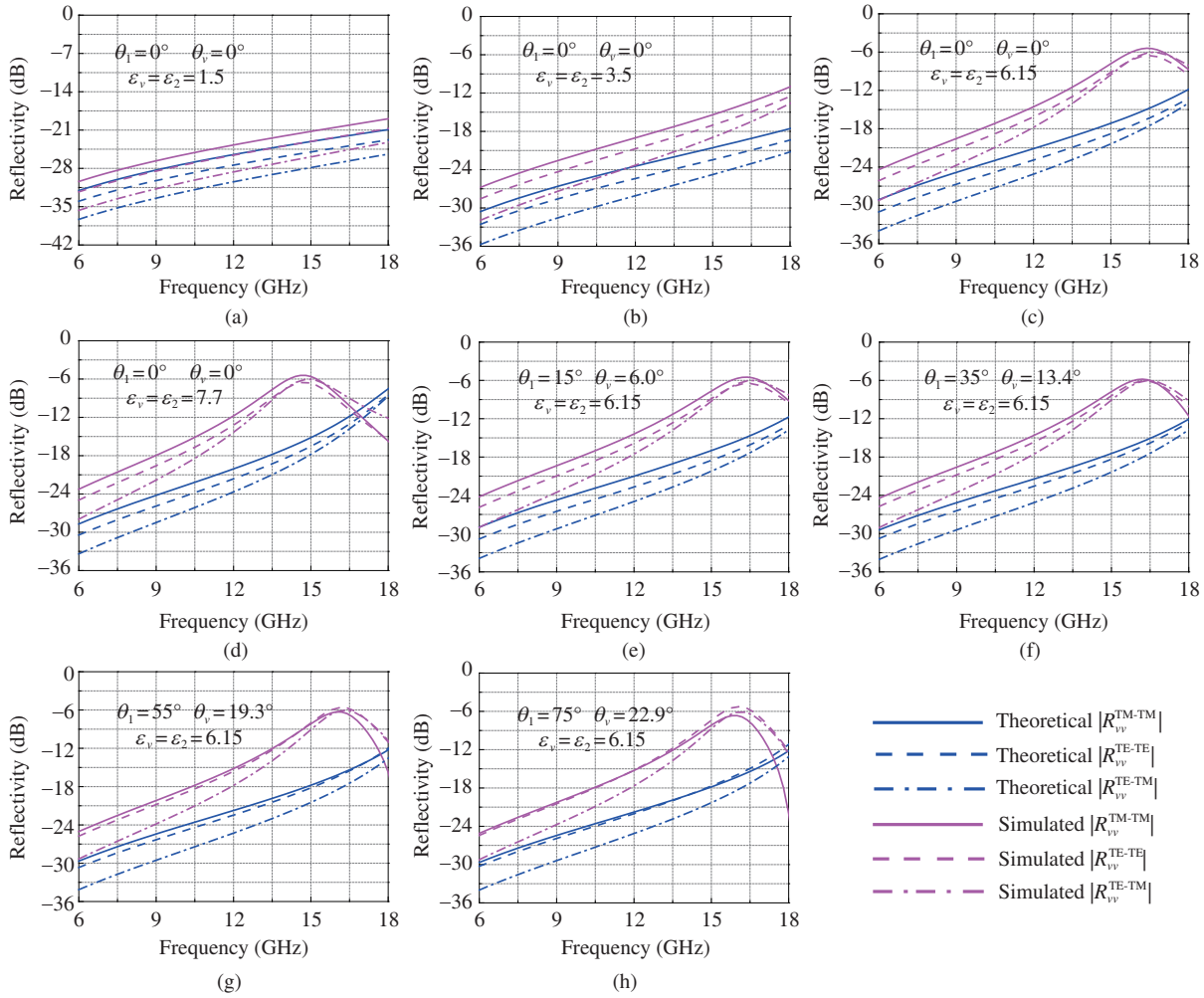

Figure 9 (Color online) Theoretical and simulated reflection coefficients for the virtual substrate with relative permittivity of $\varepsilon_v = \varepsilon_2$: (a)–(d) at normal incidence with varying substrate 2 and (e)–(h) at oblique incidence with fixed substrate 2.

metallic elements).

Finally, for comparison, Figure 9 shows the theoretical and simulated R with a permittivity of $\varepsilon_v = \varepsilon_2$. As expected, the theoretical results deviate from the simulated ones. For example, as shown in Figure 9(a), when ε_2 is set as 1.5, there is an obvious difference between the theoretical and simulated results. The inconsistency further increases the credibility of the proposed theory for the uniqueness of virtual substrate. Only when the virtual substrate is given with specific relative permittivity, the updated model can be the same as the original one. Thus, it can be concluded that the virtual substrate is not only a mathematical limit means for the periodic metallic elements, but also has obvious physical meaning for the boundary condition.

4 Conclusion

In conclusion, the uniqueness of the zero-thickness virtual substrate is verified for periodic metallic elements in a dielectric half-space. When the zero-thickness virtual substrate is introduced at the interface of the periodic metallic elements, the updated model seems always to boil down to the original one, regardless of the relative permittivity of the virtual substrate. In order to verify whether an arbitrary virtual substrate holds, the traditional transmission line model and the tangential network transmission theory are adopted to verify the uniqueness of the zero-thickness virtual substrate for periodic isotropic and anisotropic metallic elements, respectively. The phenomenon can be interpreted as follows: the mathematical limit gives an alternative means to approach the actual physical situation, but the actual physical situation determines the way how the mathematical limit approaches it. Finally, for comparison,

two different virtual substrates were introduced to verify the proposed theory, regardless of the actual metallic elements, substrates, and incidence angles. The theory can also be used to convert the solution of periodic metallic elements in a dielectric half-space to that of the same periodic metallic elements in a uniform substrate, which can greatly simplify the theoretical analysis and design of the metasurface.

Acknowledgements This work was supported by the National Natural Science Foundation of China (Grant No. 61801366) and Natural Science Foundation of Shaanxi Province (Grant No. 2020JM-078).

References

1 Yu N, Capasso F. Flat optics with designer metasurfaces. Nat Mater, 2014, 13: 139–150
2 Li A B, Kim S, Luo Y, et al. High-power transistor-based tunable and switchable metasurface absorber. IEEE Trans Microw Theory Tech, 2017, 65: 2810–2818
3 Chen Z B, Deng H, Xiong Q, et al. Phase gradient metasurface with broadband anomalous reflection based on cross-shaped units. Appl Phys A, 2018, 124: 281
4 Lin F H, Chen Z N. Low-profile wideband metasurface antennas using characteristic mode analysis. IEEE Trans Antennas Propagat, 2017, 65: 1706–1713
5 Pfeiffer C, Zhang C, Ray V, et al. High performance bianisotropic metasurfaces: asymmetric transmission of light. Phys Rev Lett, 2014, 113: 023902
6 Ma H F, Wang G Z, Kong G S, et al. Broadband circular and linear polarization conversions realized by thin birefringent reflective metasurfaces. Opt Mater Express, 2014, 4: 1717–1724
7 Shi J H, Ma H F, Guan C Y, et al. Broadband chirality and asymmetric transmission in ultrathin 90°-twisted Babinet-inverted metasurfaces. Phys Rev B, 2014, 89: 165128
8 Guo W L, Wang G M, Li T J, et al. Ultra-thin anisotropic metasurface for polarized beam splitting and reflected beam steering applications. J Phys D-Appl Phys, 2016, 49: 425305
9 Xu J J, Zhang H C, Zhang Q, et al. Efficient conversion of surface-plasmon-like modes to spatial radiated modes. Appl Phys Lett, 2015, 106: 021102
10 Wu C J, Cheng Y C, Wang W Y, et al. Ultra-thin and polarization-independent phase gradient metasurface for high-efficiency spoof surface-plasmon-polariton coupling. Appl Phys Express, 2015, 8: 122001
11 Fan Y, Wang J F, Li Y F, et al. Frequency scanning radiation by decoupling spoof surface plasmon polaritons via phase gradient metasurface. IEEE Trans Antennas Propagat, 2018, 66: 203–208
12 Chen M L N, Jiang L J, Sha W E I. Ultrathin complementary metasurface for orbital angular momentum generation at microwave frequencies. IEEE Trans Antennas Propagat, 2017, 65: 396–400
13 Chen X M, Xue W, Shi H Y, et al. Orbital angular momentum multiplexing in highly reverberant environments. IEEE Microw Wireless Compon Lett, 2020, 30: 112–115
14 Estakhri N M, Alu A. Ultra-thin unidirectional carpet cloak and wavefront reconstruction with graded metasurfaces. Antennas Wirel Propag Lett, 2014, 13: 1775–1778
15 Yang Y H, Jing L Q, Zheng B, et al. Full-polarization 3D metasurface cloak with preserved amplitude and phase. Adv Mater, 2016, 28: 6866–6871
16 Zhao Y, Cao X Y, Gao J, et al. Broadband low-RCS metasurface and its application on antenna. IEEE Trans Antennas Propagat, 2016, 64: 2954–2962
17 Yang J J, Cheng Y Z, Ge C C, et al. Broadband polarization conversion metasurface based on metal cut-wire structure for radar cross section reduction. Materials, 2018, 11: 626
18 Gao X, Han X, Cao W P, et al. Ultrawideband and high-efficiency linear polarization converter based on double V-shaped metasurface. IEEE Trans Antennas Propagat, 2015, 63: 3522–3530
19 Fang C, Cheng Y Z, He Z Q, et al. A broadband reflective linear polarization converter based on multi-reflection interference theory. In: Proceedings of Progress in Electromagnetic Research Symposium (PIERS), 2016. 3033–3036
20 Hoppe D, Rahmat-Samii Y. Impedance Boundary Conditions in Electromagnetics. Boca Raton: CRC Press, 1995
21 Tretyakov S. Analytical Modeling in Applied Electromagnetics. Norwood: Artech House, 2003
22 Padooru Y, Yakovlev A, Chen P, et al. Analytical modeling of conformal mantle cloaks for cylindrical objects using subwavelength printed and slotted arrays. J Appl Phys, 2013, 114: 074508
23 Jiang S C, Xiong X, Hu Y S, et al. Controlling the polarization state of light with a dispersion-free metastructure. Phys Rev X, 2014, 4: 021026
24 Liu X B, Li W, Zhao Z Z, et al. Tangential network transmission theory of reflective metasurface with obliquely incident plane waves. IEEE Trans Microw Theory Tech, 2018, 66: 64–72
25 Vahabzadeh Y, Chamanara N, Caloz C. Generalized sheet transition condition FDTD simulation of metasurface. IEEE Trans Antennas Propagat, 2018, 66: 271–280
26 Luukkonen O, Simovski C, Granet G, et al. Simple and accurate analytical model of planar grids and high-impedance surfaces comprising metal strips or patches. IEEE Trans Antennas Propagat, 2008, 56: 1624–1632
27 Liu X B, Zhang J S, Chen X M, et al. A generalized accurate model for complementary periodic subwavelength metasurface based on babinet principle. IEEE Trans Antennas Propagat, 2020, 68: 3780–3790